EDGE ARTICLE

CrossMark
← click for updates

Shape and composition control of $Bi_{19}S_{27}(Br_{3-x},I_x)$ alloyed nanowires: the role of metal ions†

Yihui Wu,[a] Huanhuan Pan,[b] Xin Zhou,[a] Mingrun Li,[a] Bin Zhou,[a] Chi Yang,[ac] Wen-Hua Zhang,*[a] Jiansheng Jie*[b] and Can Li*[a]

We present the first colloidal synthesis of highly uniform single-crystalline $Bi_{19}S_{27}Br_3$ nanowires (NWs) with a mean diameter of ~9 nm and tunable lengths in the range of 0.15–2 μm in the presence of foreign metal ions (Al^{3+}). The Al^{3+} ions not only control the growth of NWs, but also achieve species transformation, *i.e.*, from Bi_2S_3 to $Bi_{19}S_{27}Br_3$, and are not present in the resulting NWs. This colloidal chemistry approach can be expanded to prepare a family of single-crystalline $Bi_{19}S_{27}(Br_{3-x},I_x)$ alloyed NWs with controlled compositions ($0 \leq x \leq 3$). Interestingly, these alloyed NWs show an unusual composition-independent band gap of ~0.82 eV, and theoretical calculations indicate that this phenomenon comes from the very minor contributions of the halogens to the valence band maximum and conduction band minimum. The photodetectors made of $Bi_{19}S_{27}(Br_{3-x},I_x)$ alloyed NWs show a pronounced photoresponse with high stability and reproducibility, which makes the NWs potentially useful candidates in optoelectronic devices.

Introduction

Semiconductor nanowires (NWs),[1] which are key building blocks for the next generation of optoelectronic devices such as light-emitting diodes (LEDs),[2] solar cells,[3] photodetectors,[4] field-effect transistors (FETs),[5] thermoelectric devices[6] and so on, have been extensively studied due to their anisotropic geometry, large surface-to-volume ratio, their decoupling of light absorption and minority carrier diffusion directions for efficient charge collection and separation, and their exciton confinement in two dimensions that are superior to their bulk counterparts. Moreover, semiconductor NWs have various mechanical properties and reactivities which depend on the crystallographic orientation.[7] Considerable efforts have been made to exploit their useful properties and widen their applications, and especially to improve their synthesis[1a,8] by metal-nanoparticle-mediated methods,[9] direct deposition methods,[10] template-directed methods,[11] and oriented-attachment methods in colloidal chemistry.[12] Colloidal synthesis, which takes advantage of the versatility of the precursors, ligand affinity, solvent polarity, and reaction parameters, has been demonstrated to be a powerful strategy for exploiting colloidal nanocrystals (NCs) with controlled phases,[13] morphology[14] and composition[15] for binary and ternary systems. The superiority of colloidal chemistry has also been demonstrated in the synthesis of very interesting semiconducting heterostructured NCs.[16] In contrast, the controllable synthesis of quaternary and quinary alloyed NCs is much more difficult, and the synthesis of multi-component NWs is an even bigger challenge than nanoparticles. Generally, long carbon chain organic molecules that selectively bind to different NC facets are used to control the morphology of the resulting NCs.[17] More recently, inorganic foreign metal ions have been employed to influence the morphology of semiconductor NCs (Cu_xSe and CuTe NCs),[18] which may provide a new way to control the shape of NCs. However, no success has been reported on the formation of one-dimensional nanomaterials mediated by foreign metal ions up to date, let alone multi-component NWs. This inspired us to employ this strategy to exploit a new type of multi-component semiconductor NW, which may greatly expand the research platform in this field.

A group of $Bi^{III}VI^AVII^A$ compounds, BiOCl, BiSCl, $Bi_{19}S_{27}Br_3$, and BiSI, has provoked great research interest varying from catalysis to electronics due to their promising properties, such as their optoelectronic effect, photoconductivity, ferroelectricity, piezoelectricity, electromechanical effect, and a large temperature dependence of the band gap.[19] Traditionally, these semiconductors with poorly defined morphology were synthesized *via* vapor-phase growth at high temperature (>600 °C), which usually required specialized and complicated facilities and even toxic H_2S and HBr.[20] Solvothermal methods have been

[a] State Key Laboratory of Catalysis, Dalian Institute of Chemical Physics, Chinese Academy of Sciences, Dalian National Laboratory for Clean Energy, Dalian 116023, China. E-mail: whzhang@dicp.ac.cn; canli@dicp.ac.cn

[b] Institute of Functional Nano & Soft Materials (FUNSOM), Collaborative Innovation Center of Suzhou Nano Science and Technology, Soochow University, Suzhou, Jiangsu 215123, China. E-mail: jsjie@suda.edu.cn

[c] Department of Materials Science and Engineering, University of Science and Technology of China, Hefei 230026, China

† Electronic supplementary information (ESI) available: Experimental details, XRD patterns, TEM and HRTEM images, energy-dispersive X-ray spectra, UV-vis spectra, and Tauc plots. See DOI: 10.1039/c5sc00708a

exploited to prepare bundle–rod-like $Bi_{19}S_{27}Br_3$.[19c] A microwave-assisted aqueous synthesis has recently been developed to prepare fabric-like $Bi_{19}S_{27}Br_3$ superstructures with large diameters (~80 nm) and their photocatalytic performance has also been investigated.[19d] However, to the best of our knowledge, the controllable synthesis of single-crystalline $Bi_{19}S_{27}Br_3$ colloidal NWs with uniform morphology remains undeveloped, hindering the understanding of their fundamental properties and the exploitation of their potential applications. Herein we present a facile, colloidal approach to well-defined $Bi_{19}S_{27}Br_3$ NWs by using Al^{3+} ions to mediate the oriented growth of $Bi_{19}S_{27}Br_3$. We have demonstrated that aluminium(III) acetylacetonate $[Al(acac)_3]$ not only controls the growth of NWs, but also achieves species transformation, i.e., from Bi_2S_3 to $Bi_{19}S_{27}Br_3$. We have further expanded this foreign metal ion mediated approach to realize the synthesis of uniform quaternary $Bi_{19}S_{27}(Br_{3-x},I_x)$ NWs with compositions varying across the entire range ($0 \leq x \leq 3$). Full experimental details can be found in the ESI.† Their microstructures and properties were thoroughly characterized by a variety of analyses, such as X-ray diffraction (XRD), X-ray photoelectron spectroscopy (XPS), Raman spectra, scanning electron microscopy (SEM), transmission electron microscopy (TEM), high-resolution transmission electron microscopy (HRTEM), and UV-visible-near-infrared (UV-vis-NIR) absorption spectroscopy. It is very interesting to find that these alloyed NWs show an unusual composition-independent band gap, which differs from the widely accepted Vegard's law for multi-component alloyed semiconductors.[21] The application potential of $Bi_{19}S_{27}(Br_{3-x},I_x)$ NWs in photoelectronics was finally assessed by fabricating photodetectors (PDs), showing a pronounced photoresponse with high stability.

Results and discussion

Fig. 1a shows the TEM image of the sample prepared in the absence of Al^{3+}. The product was assembled from fabric-like NWs with a wide range of diameters, and was revealed to be orthorhombic Bi_2S_3 (JCPDS no. 17-0320) by XRD (Fig. 1d). The high-angle annular dark-field-scanning transmission microscopy (HAADF-STEM) and TEM image reveals the fabric-like morphology of Bi_2S_3 should be formed via physical crossover of non-uniform NWs (Fig. S1, ESI†). High resolution TEM (HRTEM) images along with the corresponding fast Fourier transform (FFT) pattern confirm the single crystalline nature of the product (Fig. S1, ESI†). Very interestingly, the presence of $Al(acac)_3$ in the synthesis medium resulted in hexagonal-structured $Bi_{19}S_{27}Br_3$ NWs (JCPDS no. 26-0813) with mean diameters of ~9.0 nm, as shown in Fig. 1b (TEM) and Fig. 1d (XRD). It is noteworthy that the length of the as-synthesized $Bi_{19}S_{27}Br_3$ NWs can be tuned in the range of 0.15–2 μm by varying the reaction duration while the mean diameters do not appear to change (Fig. S2, ESI,† the reaction temperature was kept at 180 °C). Moreover, the mean diameters can be tuned from ~6.9 nm to ~12 nm by varying the reaction temperature while the length of the NWs remain basically unchanged (Fig. S3, ESI,† the reaction time was kept at 30 min). Therefore, the presence of $Al(acac)_3$

was critical for the formation of $Bi_{19}S_{27}Br_3$ NWs and the reaction conditions were important to produce NWs with narrow size distributions. To ascertain whether it is the Al^{3+} that plays the key role in the formation of the well-defined $Bi_{19}S_{27}Br_3$ NWs, $AlCl_3$ was used as additive to replace $Al(acac)_3$ in the synthesis process. Hexagonal $Bi_{19}S_{27}Br_3$ NWs with very similar morphologies were again obtained (Fig. 1c and d), as in the case of $Al(acac)_3$. Therefore, Al^{3+} ions can achieve not only morphological control, but also species transformation, i.e., from Bi_2S_3 to $Bi_{19}S_{27}Br_3$ in this case. To investigate the NW composition, energy dispersive X-ray spectroscopy (EDS) was performed (Table S1, ESI†), showing the ratio of Bi : S : Br was approximately 19 : 26 : 5. Thus the as-synthesized NWs are slightly sulfur poor and bromine rich. However, EDS cannot detect the presence of any Al element in the NWs. X-ray photoelectron spectroscopy (XPS) was further employed to characterize the $Bi_{19}S_{27}Br_3$ NWs (Fig. 2), displaying peaks centred at 158.4 eV and 163.7 eV, which corresponded to the Bi $4f_{7/2}$ and Bi $4f_{5/2}$ of the Bi^{3+} ions,[22] respectively. The peaks centred at 161.1 eV and 162.2 eV overlapping with Bi 4f were assigned to S $2p_{3/2}$ and S $2p_{1/2}$ of the S^{2-} ions,[22b,23] respectively. The signal with binding energy of 68.4 eV is characteristic of Br^- ions (Br 3d). Altogether, the above data confirm that the $Bi_{19}S_{27}Br_3$ NWs obtained through our colloidal approach are phase pure.

The influence of the concentration of Al^{3+} ions on the dimension of the resulting $Bi_{19}S_{27}Br_3$ NWs was further studied by adding different amounts of Al^{3+} ions in the synthesis. It was found that the length of the $Bi_{19}S_{27}Br_3$ NWs gradually decreased to a certain degree upon increasing the dosage of Al^{3+} ions, while the mean diameters of the $Bi_{19}S_{27}Br_3$ NWs remained constant (Fig. S4, ESI†). The role of Al^{3+} ions in the shape
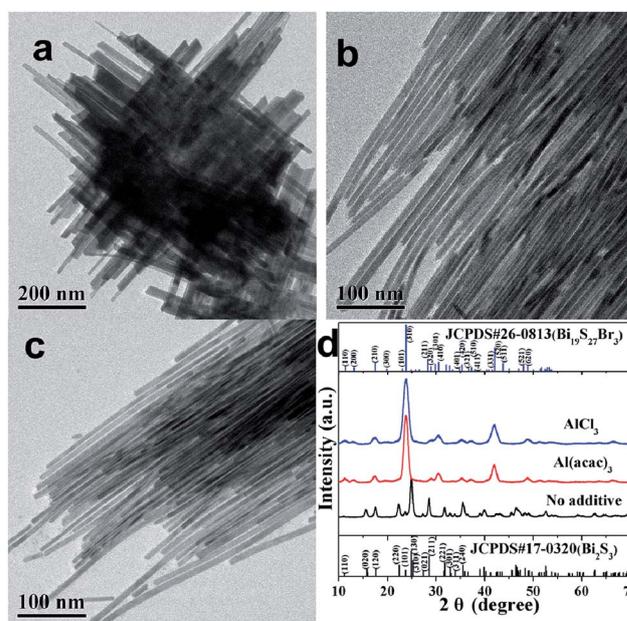

Fig. 1 TEM images of the as-synthesized NWs obtained by adding different salts into the reaction mixtures: (a) no additive, (b) $Al(acac)_3$, (c) $AlCl_3$, and (d) the corresponding XRD patterns of the three materials.

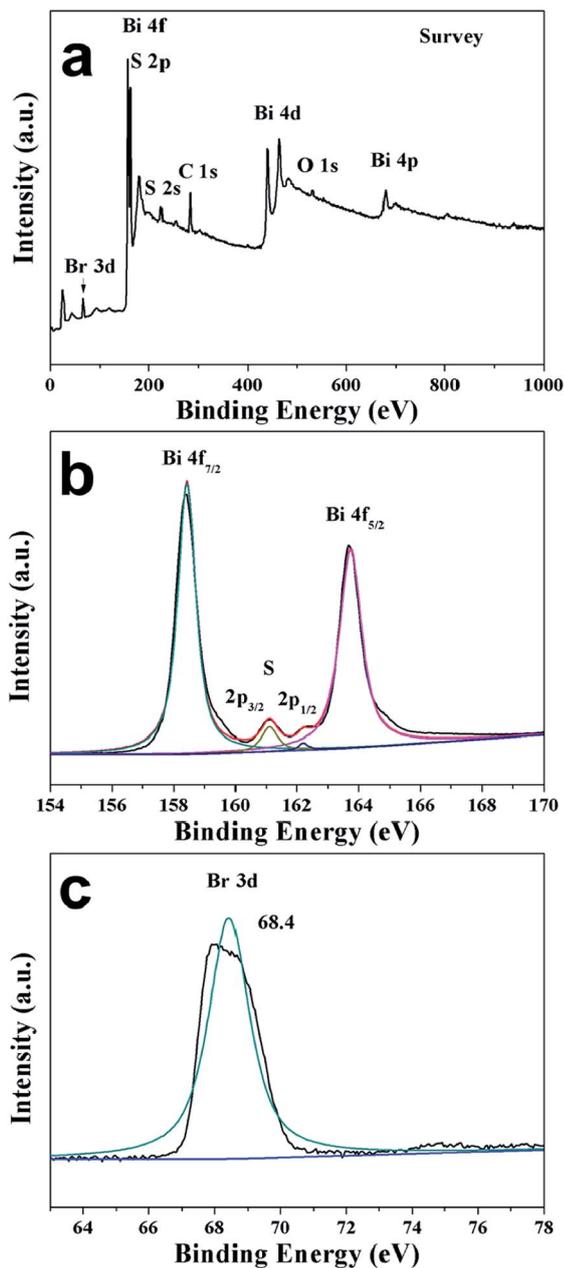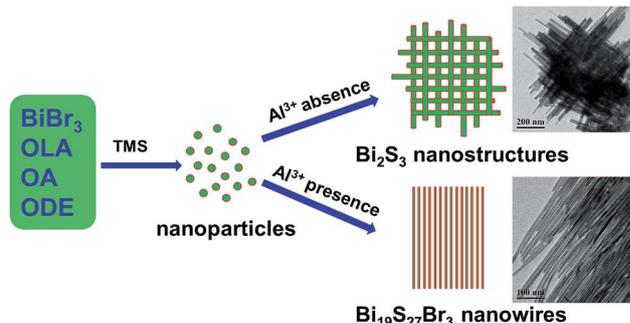**Fig. 2** XPS spectra of $Bi_{19}S_{27}Br_3$ NWs: (a) survey XPS spectrum, (b) high-resolution spectra of Bi 4f and S 2p, and (c) high-resolution spectrum of Br 3d.

is that, during the NW synthesis, $BiBr_3$ and $Al(acac)_3$ simultaneously dissolve in the ODE solution, where they should exist in molecular form. $BiBr_3$ molecules may be surrounded by some Al^{3+} *via* the electrostatic force between Br^- and Al^{3+}. In such a case, Al^{3+} can form a screen to suppress, to a certain degree, the attack of S^{2-} to $BiBr_3$, thus a portion of Br^- is retained as a reaction intermediate, leading to the formation of a new species $Bi_{19}S_{27}Br_3$. Deep understanding of the growth process is very complicated and further study should be performed with the aid of theoretical calculations. If any of the above explanations are true, it could be expected that other cations should also exert a similar influence on the reaction of nanowire growth in this study. Hence we chose Fe^{3+}, Fe^{2+}, Co^{3+}, Co^{2+}, and Ni^{2+} ions to investigate the influence of foreign metal ions on this reaction. Indeed, these cations function almost the same as Al^{3+} ions in the formation of $Bi_{19}S_{27}Br_3$. The corresponding TEM images and XRD patterns for these nanowires are shown in Fig. S5 and S6, ESI,† respectively.

To expand the present synthesis of $Bi_{19}S_{27}Br_3$ NWs to other $Bi^{III}VI^AVII^A$ materials, we further prepared $Bi_{19}S_{27}(Br_{3-x},I_x)$ ($0 \leq x \leq 3$) alloyed NWs. Fig. 3a presents the XRD patterns of the as-synthesized $Bi_{19}S_{27}(Br_{3-x},I_x)$ NWs ($0 \leq x \leq 3$). For $Bi_{19}S_{27}I_3$, the XRD pattern does not match any existing patterns in the standard JCPDS database, thus a diffraction pattern for hexagonal $Bi_{19}S_{27}I_3$ was simulated on the basis of $Bi_{19}S_{27}Br_3$ crystal structure by substituting the Br^- lattice positions with I^- (Table S2, ESI†). The lattice constants calculated from the experimental diffraction pattern ($a = 15.65$ Å and $c = 4.026$ Å) were used in this simulation. The d-spacings of the experimental reflections match well with the simulated ones, indicating that $Bi_{19}S_{27}I_3$ NWs should exhibit the same hexagonal structure as $Bi_{19}S_{27}Br_3$ NWs. Additionally, the major diffraction peaks shift systematically towards lower angles as the content of I increases, meaning that the larger I atoms have gradually replaced the smaller Br atoms in the lattices of the resulting NWs. More importantly, no additional peaks or peak splitting can be detected by XRD, ruling out the possibility of phase separation or separation nucleation that often occurs in the preparation of alloyed nanocrystals.[21b] Vegard's graph (Fig. 3b), obtained by plotting the lattice parameter values (a and c) *versus* composition, shows a near-linear trend with increasing iodide

control of the $Bi_{19}S_{27}Br_3$ NWs is probably to promote crystal growth in a specific direction;[18b] the corresponding growth mechanisms of the NWs are shown in Scheme 1. If more Al^{3+} ions are present in the reaction mixture, the Bi precursors are divided into more regions, and more nucleation sites will be generated, resulting in the formation of shorter NWs. However, the transformation mechanism from Bi_2S_3 to $Bi_{19}S_{27}Br_3$ needs to be elucidated in this study. It is proposed that Al^{3+} competes with Bi^{3+} in adsorbing S^{2-} in the reaction system, which reduces the reaction probability between Bi^{3+} and S^{2-}, leading to an incomplete replacement of Br^- by S^{2-}, thus forming the hexagonal-structured $Bi_{19}S_{27}Br_3$. Another possible explanation

Scheme 1 Schematic illustration for the proposed formation process of $Bi_{19}S_{27}Br_3$ nanowires (OLA: oleylamine, OA: oleic acid, ODE: 1-octadecene).

content, confirming the formation of a solid solution. Raman spectroscopy is a sensitive tool that reflects the phase purity of a material. The Raman spectra of the as-prepared NWs in Fig. S7, ESI† show five peaks, located at 127, 145, 192, 217 and 270 cm^{-1}. The strongest Raman peak at ~270 cm^{-1} can be assigned to the motion between the Bi and S atoms as well as the Br atom at rest for the $Bi_{19}S_{27}Br_3$ NW. The absence of any Bi_2S_3 signals[24] around 185, 236 and 260 cm^{-1} and any $BiBr_3$ peaks[25] around 143, 156 and 173 cm^{-1} confirmed the high purity of the $Bi_{19}S_{27}Br_3$ NWs obtained in this study. Similar scenarios were observed for the other three samples with varied I/Br ratios. Therefore, we have successfully synthesized pure phase $Bi_{19}S_{27}(Br_{3-x},I_x)$ NWs with chemical compositions can be consecutively tailored across the entire composition range ($0 \leq x \leq 3$).

TEM and SEM were then performed to reveal the morphology and microstructures of the $Bi_{19}S_{27}(Br_{3-x},I_x)$ alloyed NWs, as shown in Fig. 4 and S8, ESI,† respectively. The low-magnification TEM and SEM images display uniform diameter distributions of the $Bi_{19}S_{27}(Br_{3-x},I_x)$ NWs, and the diameters increase gradually from ~9.0 to ~13.9 nm with as the I content increases (Fig. S9, ESI†). It is well-known that, to decrease the system energy, facets with lower energy will gradually grow larger, while the facets with higher energy gradually get smaller and even disappear during crystal growth. To gain insight into the variation in the diameters of the $Bi_{19}S_{27}(Br_{3-x},I_x)$ NWs in this study, theoretical evaluation of the surface energies of the NW facets

was carried out. The diameters of the hexagonal $Bi_{19}S_{27}(Br_{3-x},I_x)$ NWs should be influenced significantly by the relative surface energies of the (110) facet/(001) facet. This is estimated to be 2.34 for the $Bi_{19}S_{27}I_3$ NWs, which is significantly higher than the 0.71 for the $Bi_{19}S_{27}Br_3$ NWs. This means that, in comparison with the $Bi_{19}S_{27}Br_3$ NWs, the $Bi_{19}S_{27}I_3$ NWs with larger (001) facets exhibit lower system energy. The (001) facet of the $Bi_{19}S_{27}I_3$ would grow larger while the (110) facet becomes smaller. Therefore, the diameters of the $Bi_{19}S_{27}(Br_{3-x},I_x)$ NWs increase gradually when the I content is increased. High-resolution TEM (HRTEM) images show that all the $Bi_{19}S_{27}(Br_{3-x},I_x)$ NWs are highly crystalline with continuous lattice fringes and the corresponding fast Fourier transform (FFT) pattern of a single NW confirm their single crystalline nature. The lattice distance of 0.201 nm matches well with the (002) plane of the hexagonal $Bi_{19}S_{27}Br_3$, indicating that the growth of the NWs is oriented along the [001] direction. Moreover, the interplanar crystal spacing of d_{440} increases from 0.194 nm to 0.200 nm with increasing I content, meaning again that the larger I atoms have successfully replaced the smaller Br atoms in the lattices of the resulting NWs, which is in good agreement with the XRD results. Elemental analysis by EDS (Table S1 and Fig. S10, ESI†) shows that an increase in the I content was accompanied by a decrease in the Br content in the range of $0 \leq x \leq 3$ for the as-prepared $Bi_{19}S_{27}(Br_{3-x},I_x)$ NWs. Moreover, elemental mapping and a line scan (Fig. 5) of the $Bi_{19}S_{27}(BrI_2)$ NWs confirm the homogeneous distribution of the four elements present. These results demonstrate the formation of alloyed NWs with a homogeneous distribution of Br and I in the $Bi_{19}S_{27}(Br_{3-x},I_x)$ matrix.

The UV-vis-NIR diffuse-reflectance spectroscopy (DRS) spectra of the $Bi_{19}S_{27}(Br_{3-x},I_x)$ NWs ($0 \leq x \leq 3$) were measured to study their optical properties (Fig. 6a). A continuous strong absorption spanning the whole visible to near IR spectrum was found. It is noteworthy that the absorption intensity increases gradually as the I content increases. Tauc plots (Fig. S11, ESI†) were derived to determine the optical band gaps with the relationship of α^2 plotted against the energy revealing that the $Bi_{19}S_{27}Br_3$ NWs have a direct band gap of 0.815 eV. Interestingly, the band gap energies were basically unchanged upon varying the ratio of I/Br for the $Bi_{19}S_{27}(Br_{3-x},I_x)$ NWs ($0 \leq x \leq 3$), meaning that the synthesized NWs exhibited band gaps independent of the composition, which is very different from the widely accepted Vegard's law for multi-component alloyed semiconductors.[21] In order to deeply understand the electronic structure of $Bi_{19}S_{27}Br_3$, density functional theory calculations were performed with the Vienna *ab initio* simulation package[26] and a projector augmented wave method.[27] The generalized gradient approximation (GGA) with the spin polarized Perdew–Burke–Ernzerhof (PBE) functional[28] was used to relax the structure and compute the density of states. The results in Fig. 7 and S12, ESI,† show that the valence band maximum of $Bi_{19}S_{27}Br_3$ and $Bi_{19}S_{27}I_3$ is mostly composed of S 3p states and that the conduction band minimum mainly consists of Bi 6p states, slightly mixed with S 3p orbitals. In contrast, Br 4p or I 5p orbitals make important contributions to the lower region of the valence band (lower than −0.4 eV), which is possibly why the
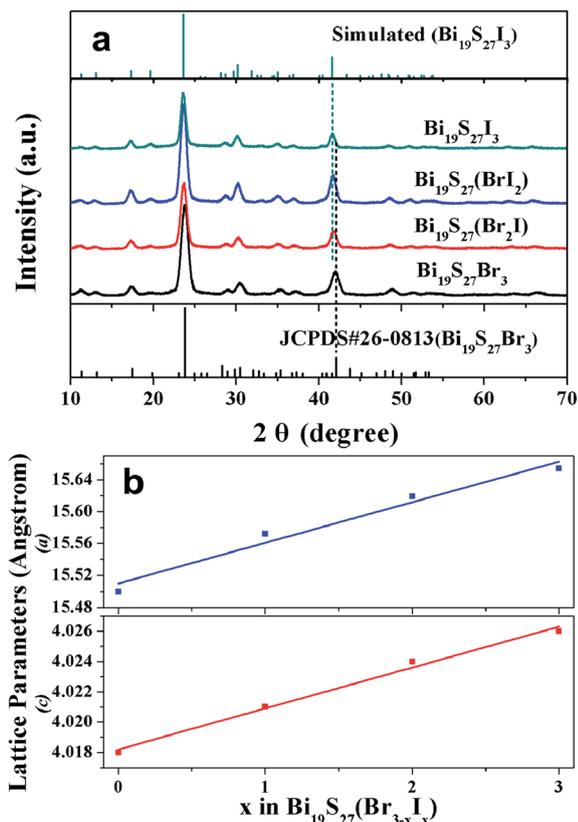

Fig. 3 XRD patterns (a) and Vegard's plot (b) of $Bi_{19}S_{27}(Br_{3-x},I_x)$ with various I/(Br + I) ratios ($0 \leq x \leq 3$).

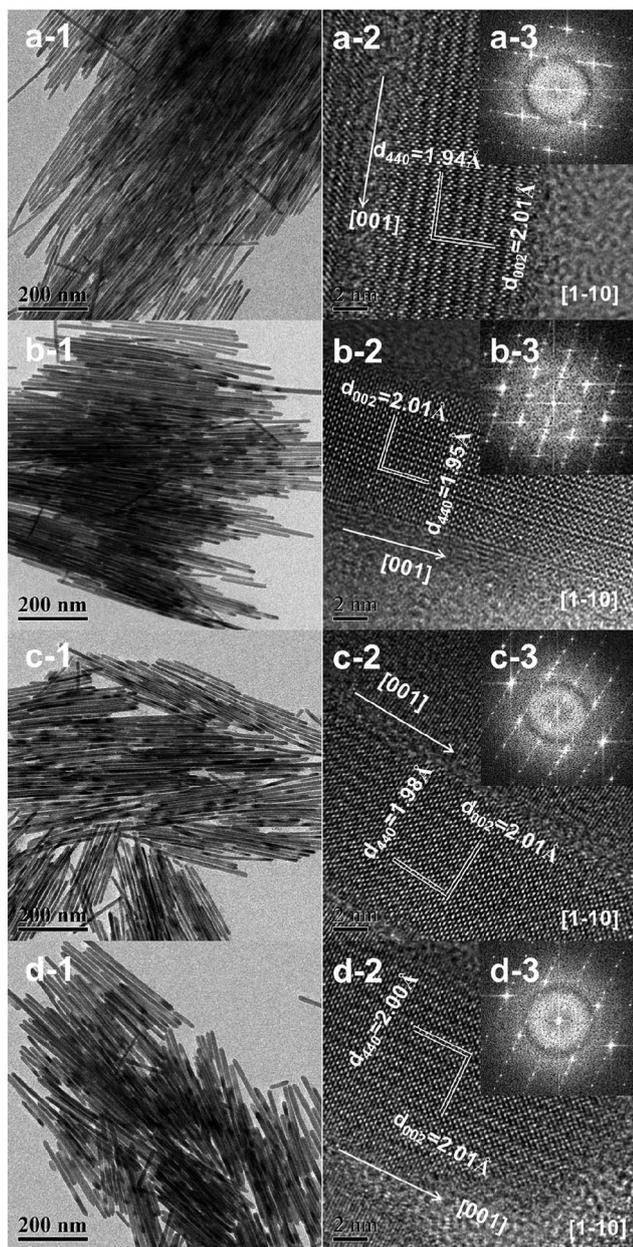**Fig. 4** TEM analysis of the $Bi_{19}S_{27}(Br_{3−x},I_x)$ ($0 ≤ x ≤ 3$) NWs. (a)–(d) Denote respectively the $Bi_{19}S_{27}Br_3$, $Bi_{19}S_{27}(Br_2I)$, $Bi_{19}S_{27}(BrI_2)$, and $Bi_{19}S_{27}I_3$ NWs. 1, 2, and 3 represent the corresponding low magnification TEM images, HRTEM images and corresponding FFT patterns for these samples, respectively.
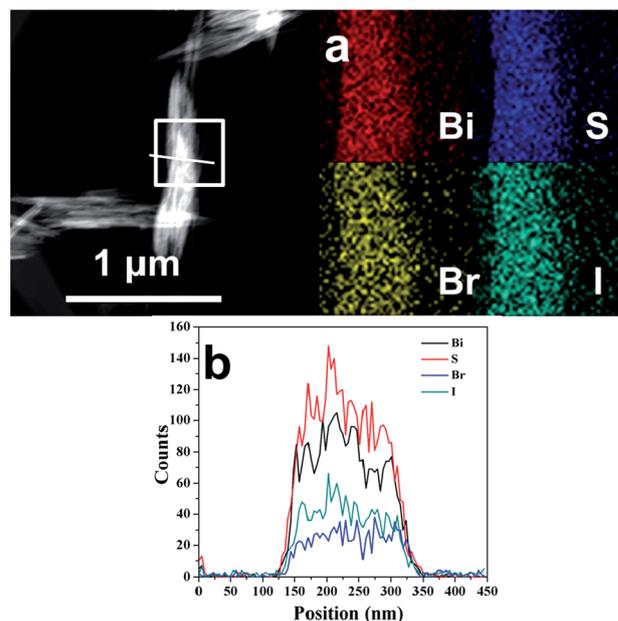

Fig. 5 HAADF-STEM image and corresponding EDS elemental mapping (a) and STEM-EDS line scan (b) of the $Bi_{19}S_{27}(BrI_2)$ NWs.

(cathode current) (Fig. 6b), indicating that the as-synthesized NWs exhibit p-type semiconductor behavior.[29] A constant bias experiment enables a more realistic evaluation of the charge transport dynamics for device applications. We hence carried out such a measurement. As shown in Fig. S13, ESI,† the photocurrents of the $Bi_{19}S_{27}(Br_{3−x},I_x)$ NW films increased rapidly upon receiving illumination, and dropped immediately to their pre-illumination values without apparent degradation over many light on/off cycles. It can also be seen that the photocurrents increased gradually with increasing content of I, which may be due to the enhanced absorption intensities, as shown in Fig. 6a. Therefore, the $Bi_{19}S_{27}(Br_{3−x},I_x)$ NWs ($0 ≤ x ≤ 3$) are sensitive to light illumination and are stable under experimental conditions, which is vital for device applications.

The combination of a strong absorption ability in the visible to near IR region of the spectrum and a sensitive response to light illumination makes the $Bi_{19}S_{27}(Br_{3−x},I_x)$ NWs ($0 ≤ x ≤ 3$) excellent candidates for photodetectors (PDs). The as-synthesized alloyed NWs were directly drop-casted on a pre-prepared
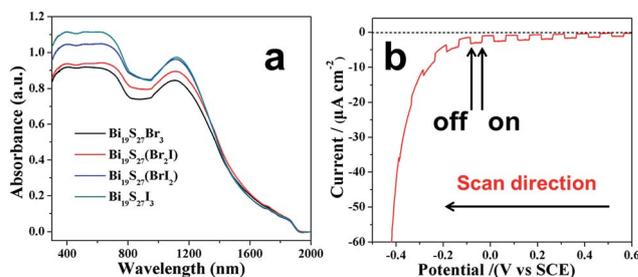
replacement of Br with I does not change the band gap of the as-synthesized NWs. The calculated band gap (about 0.6 eV) is smaller than our experimental value (around 0.82 eV) which may be due to shortcomings of the GGA method in underestimating the band gap.

We also investigated the photoelectrochemical (PEC) properties of the $Bi_{19}S_{27}(Br_{3−x},I_x)$ NWs ($0 ≤ x ≤ 3$) by measuring the transient photocurrents of the NW films on fluorine tin oxide (FTO) in a photoelectrochemical cell. The photocurrent obtained from a $Bi_{19}S_{27}(Br_2I)$ NW electrode was negative

Fig. 6 (a) UV-vis-NIR diffuse-reflectance spectra (DRS) of the $Bi_{19}S_{27}(Br_{3−x},I_x)$ ($0 ≤ x ≤ 3$) NWs, (b) transient photocurrent response of the $Bi_{19}S_{27}(Br_2I)$ NWs.

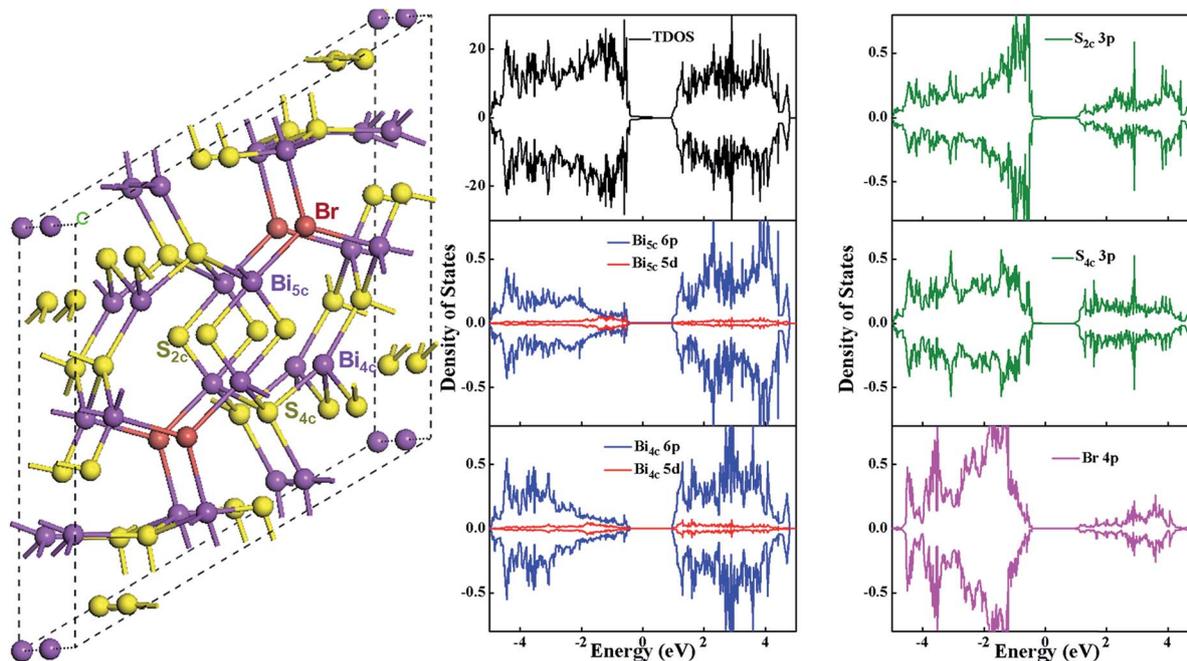**Fig. 7** The structural model and DOS for $Bi_{19}S_{27}Br_3$.

Au electrode (50 nm) paired onto a SiO_2 (300 nm)/p^+-Si substrate. Fig. 8a shows this as a schematic illustration and also a representative SEM image of the PD based on the NW network. Despite the short length and small diameter of the NWs, the NWs in the network can connect successfully both to each other and across the electrode pairs. Current *versus* voltage ($I–V$) curves of the four kinds of PDs measured in the dark are plotted in Fig. S14, ESI.† The linear shape of the curves demonstrates the ohmic contact of the NW networks with the Au electrodes. Significantly, under white light illumination (60 mW cm^{-2}), all the devices show pronounced photoresponses (Fig. 8b), and the devices could be reversibly switched between low- and high-conduction states when the light was switched off and on repeatedly, revealing the high stability and reproducibility of the PDs. Close investigation of the on/off curves reveals

that the highest photocurrent for the PDs increases with increasing iodide content (Fig. 8c), which is in good agreement with the PEC measurements. These results confirm the good optoelectronic properties of our NWs.

Conclusions

In summary, we have developed a facile solution-based method for the synthesis of highly uniform single-crystalline $Bi_{19}S_{27}$-(Br_{3-x},I_x) alloyed NWs across the whole composition range ($0 \leq x \leq 3$) with the aid of foreign metal ions (Al^{3+}). A systematic increase in the lattice constant values upon substitution of I^- for Br^- in $Bi_{19}S_{27}Br_3$ confirms the formation of $Bi_{19}S_{27}(Br_{3-x},I_x)$ alloyed NWs. The as-synthesized NWs show an unusual composition-independent band gap of ~0.82 eV which is

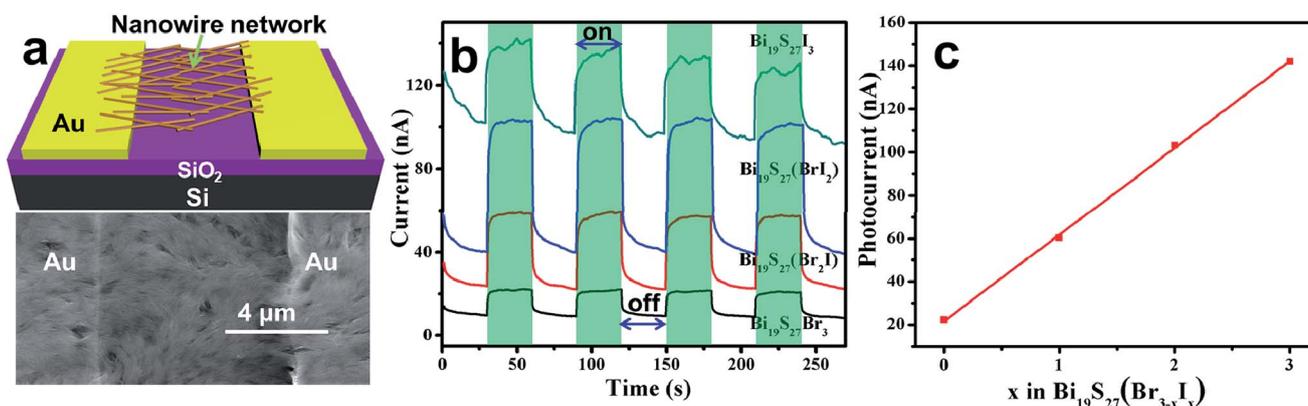**Fig. 8** (a) Schematic illustration of the PDs based on $Bi_{19}S_{27}(Br_{3-x},I_x)$ NW networks (x = 0, 1, 2, 3). SEM image of a typical device is shown below. (b) Transient photoresponse of the PDs to pulsed incident light at a bias of +5 V. (c) Photocurrent *versus* iodide content (x) curve.

mainly due to the small contributions of the halogens to the valence band maximum and conduction band minimum. Photoelectrochemical measurements reveal that the $Bi_{19}S_{27}(Br_{3-x},I_x)$ NWs are p-type semiconductors and sensitive to light irradiation. Moreover, PDs made of these NWs exhibit high sensitivity to white light, confirming the great potential of $Bi_{19}S_{27}(Br_{3-x},I_x)$ NWs in high-performance optoelectronic devices.

Acknowledgements

Notes and references

1 (a) N. P. Dasgupta, J. Sun, C. Liu, S. Brittman, S. C. Andrews, J. Lim, H. Gao, R. Yan and P. Yang, *Adv. Mater.*, 2014, **26**, 2137; (b) A. I. Hochbaum and P. Yang, *Chem. Rev.*, 2010, **110**, 527.

2 F. Qian, S. Gradečak, Y. Li, C.-Y. Wen and C. M. Lieber, *Nano Lett.*, 2005, **5**, 2287.

3 (a) T. J. Kempa, R. W. Day, S.-K. Kim, H.-G. Park and C. M. Lieber, *Energy Environ. Sci.*, 2013, **6**, 719; (b) S. Liu, X. Guo, M. Li, W.-H. Zhang, X. Liu and C. Li, *Angew. Chem., Int. Ed.*, 2011, **50**, 12050.

4 (a) J. Miao, W. Hu, N. Guo, Z. Lu, X. Zou, L. Liao, S. Shi, P. Chen, Z. Fan, J. C. Ho, T.-X. Li, X. S. Chen and W. Lu, *ACS Nano*, 2014, **8**, 3628; (b) G. Chen, B. Liang, X. Liu, Z. Liu, G. Yu, X. Xie, T. Luo, D. Chen, M. Zhu, G. Shen and Z. Fan, *ACS Nano*, 2014, **8**, 787; (c) J.-J. Wang, Y.-Q. Wang, F.-F. Cao, Y.-G. Guo and L.-J. Wan, *J. Am. Chem. Soc.*, 2010, **132**, 12218.

5 L. Li, H. Lu, Z. Yang, L. Tong, Y. Bando and D. Golberg, *Adv. Mater.*, 2013, **25**, 1109.

6 H. Fang, T. Feng, H. Yang, X. Ruan and Y. Wu, *Nano Lett.*, 2013, **13**, 2058.

7 E. W. Wong, P. E. Sheehan and C. M. Lieber, *Science*, 1997, **277**, 1971.

8 Y. Xia, P. Yang, Y. Sun, Y. Wu, B. Mayers, B. Gates, Y. Yin, F. Kim and H. Yan, *Adv. Mater.*, 2003, **15**, 353.

9 (a) G. Meng, T. Yanagida, K. Nagashima, H. Yoshida, M. Kanai, A. Klamchuen, F. Zhuge, Y. He, S. Rahong, X. Fang, S. Takeda and T. Kawai, *J. Am. Chem. Soc.*, 2013, **135**, 7033; (b) M. Heurlin, M. H. Magnusson, D. Lindgren, M. Ek, L. R. Wallenberg, K. Deppert and L. Samuelson, *Nature*, 2012, **492**, 90; (c) H.-Y. Tuan, D. C. Lee and B. A. Korgel, *Angew. Chem., Int. Ed.*, 2006, **45**, 5184.

10 (a) J. Joo, B. Y. Chow, M. Prakash, E. S. Boyden and J. M. Jacobson, *Nat. Mater.*, 2011, **10**, 596; (b) F. Meng, S. A. Morin and S. Jin, *J. Am. Chem. Soc.*, 2011, **133**, 8408.

11 (a) C. Wang, Y. Hu, C. M. Lieber and S. Sun, *J. Am. Chem. Soc.*, 2008, **130**, 8902; (b) J. Tang, Z. Huo, S. Brittman, H. Gao and P. Yang, *Nat. Nanotechnol.*, 2011, **6**, 568.

12 (a) C. O'Sullivan, R. D. Gunning, A. Sanyal, C. A. Barrett, H. Geaney, F. R. Laffir, S. Ahmed and K. M. Ryan, *J. Am. Chem. Soc.*, 2009, **131**, 12250; (b) N. Pradhan, H. Xu and X. Peng, *Nano Lett.*, 2006, **6**, 720; (c) K.-S. Cho, D. V. Talapin, W. Gaschler and C. B. Murray, *J. Am. Chem. Soc.*, 2005, **127**, 7140.

13 (a) X. Zhang, N. Bao, K. Ramasamy, Y.-H. A. Wang, Y. Wang, B. Lin and A. Gupta, *Chem. Commun.*, 2012, **48**, 4956; (b) Y. Zou, X. Su and J. Jiang, *J. Am. Chem. Soc.*, 2013, **135**, 18377; (c) M. E. Norako, M. J. Greaney and R. L. Brutchey, *J. Am. Chem. Soc.*, 2012, **134**, 23.

14 (a) K. P. Rice, A. E. Saunders and M. P. Stoykovich, *J. Am. Chem. Soc.*, 2013, **135**, 6669; (b) Y.-H. A. Wang, X. Zhang, N. Bao, B. Lin and A. Gupta, *J. Am. Chem. Soc.*, 2011, **133**, 11072; (c) X. Peng, L. Manna, W. Yang, J. Wickham, E. Scher, A. Kadavanich and A. P. Alivisatos, *Nature*, 2000, **404**, 59; (d) W. Zhou, M. Yao, L. Guo, Y. Li, J. Li and S. Yang, *J. Am. Chem. Soc.*, 2009, **131**, 2959; (e) J. Nai, Y. Tian, X. Guan and L. Guo, *J. Am. Chem. Soc.*, 2013, **135**, 16082.

15 (a) C. Yang, B. Zhou, S. Miao, C. Yang, B. Cai, W.-H. Zhang and X. Xu, *J. Am. Chem. Soc.*, 2013, **135**, 5958; (b) A. Singh, S. Singh, S. Levcenko, T. Unold, F. Laffir and K. M. Ryan, *Angew. Chem., Int. Ed.*, 2013, **52**, 9120; (c) Y. Wu, B. Zhou, M. Li, C. Yang, W.-H. Zhang and C. Li, *Chem. Commun.*, 2014, **50**, 12738.

16 (a) L. Wu, B. Quan, Y. Liu, R. Song and Z. Tang, *ACS Nano*, 2011, **5**, 2224; (b) W. Han, L. Yi, N. Zhao, A. Tang, M. Gao and Z. Tang, *J. Am. Chem. Soc.*, 2008, **130**, 13152.

17 (a) J.-j. Wang, P. Liu, C. C. Seaton and K. M. Ryan, *J. Am. Chem. Soc.*, 2014, **136**, 7954; (b) Z. Li and X. Peng, *J. Am. Chem. Soc.*, 2011, **133**, 6578; (c) E. A. Weiss, *Acc. Chem. Res.*, 2013, **46**, 2607.

18 (a) W. Li, R. Zamani, P. Rivera Gil, B. Pelaz, M. Ibáñez, D. Cadavid, A. Shavel, R. A. Alvarez-Puebla, W. J. Parak, J. Arbiol and A. Cabot, *J. Am. Chem. Soc.*, 2013, **135**, 7098; (b) W. Li, R. Zamani, M. Ibáñez, D. Cadavid, A. Shavel, J. R. Morante, J. Arbiol and A. Cabot, *J. Am. Chem. Soc.*, 2013, **135**, 4664.

19 (a) Y. Wu, B. Yuan, M. Li, W.-H. Zhang, Y. Liu and C. Li, *Chem. Sci.*, 2015, **6**, 1873; (b) V. Krämer, *J. Appl. Crystallogr.*, 1973, **6**, 499; (c) L. Zhu, Y. Xie, X. Zheng, X. Yin and X. Tian, *Inorg. Chem.*, 2002, **41**, 4560; (d) C. Deng, H. Guan and X. Tian, *Mater. Lett.*, 2013, **108**, 17.

20 K. Mariolacos, *Mater. Res. Bull.*, 2004, **39**, 591.

21 (a) L. Vegard and H. Schjelderup, *Z. Phys.*, 1917, **18**, 93; (b) M. D. Regulacio and M.-Y. Han, *Acc. Chem. Res.*, 2010, **43**, 621.

22 (a) K. Ai, Y. Liu, J. Liu, Q. Yuan, Y. He and L. Lu, *Adv. Mater.*, 2011, **23**, 4886; (b) J. Grigas, E. Talik and V. Lazauskas, *Phys. Status Solidi B*, 2002, **232**, 220.

23 H. Li, Q. Zhang, A. Pan, Y. Wang, B. Zou and H. J. Fan, *Chem. Mater.*, 2011, **23**, 1299.

24 Y. Zhao, K. T. E. Chua, C. K. Gan, J. Zhang, B. Peng, Z. Peng and Q. Xiong, *Phys. Rev. B: Condens. Matter Mater. Phys.*, 2011, **84**, 205330.

25 G. A. Bowmaker, J. M. Harrowfield, P. C. Junk, B. W. Shelton and A. H. White, *Aust. J. Chem.*, 1998, **51**, 285.

26 (*a*) G. Kresse and J. Furthmüller, *Comput. Mater. Sci.*, 1996, **6**, 15; (*b*) G. Kresse and J. Furthmüller, *Phys. Rev. B: Condens. Matter Mater. Phys.*, 1996, **54**, 11169.

27 (*a*) P. E. Blöchl, *Phys. Rev. B: Condens. Matter Mater. Phys.*, 1994, **50**, 17953; (*b*) G. Kresse and D. Joubert, *Phys. Rev. B: Condens. Matter Mater. Phys.*, 1999, **59**, 1758.

28 J. P. Predew, K. Burke and M. Ernzerhof, *Phys. Rev. Lett.*, 1996, **77**, 3865.

29 D. H. Webber and R. L. Brutchey, *J. Am. Chem. Soc.*, 2012, **134**, 1085.